1 **Particulate biogenic barium tracer of mesopelagic carbon remineralization in the**

2 **Mediterranean Sea (PEACETIME project)**

4 Stéphanie H.M. Jacquet[1*], Christian Tamburini[1], Marc Garel[1], Aurélie Dufour[1], France

5 VanVambeke[1], Frédéric A.C. Le Moigne[1], Nagib Bhairy[1], Sophie Guasco[1]

7 [1]Aix Marseille Université, CNRS/INSU, Université de Toulon, IRD, Mediterranean Institute

8 of Oceanography (MIO), UM 110, 13288 Marseille, France

10 [*]Correspondence to: S. Jacquet (*stephanie.jacquet@mio.osupytheas.fr*)

13 **PEACETIME special issue**

ABSTRACT

We report on the sub-basins variability of particulate organic carbon (POC) remineralization in the western and central Mediterranean Sea during a late spring period (PEACETIME cruise). POC remineralization rates were estimated using the excess biogenic particulate barium (Ba_{xs}) inventories in mesopelagic waters (100-1000 m) and compared with prokaryotic heterotrophic production (PHP). Ba_{xs}-based mesopelagic remineralization rates (MR) range from 25 ± 2 to 306 ± 70 mg C m^{-2} d^{-1}. MR are larger in the Alger (ALG) basin compared to the Tyrrhenian (TYR) and Ionian (ION) basins. Our Ba_{xs} inventories and integrated PHP data also indicates that significant mesopelagic remineralization occurs down to 1000 m depth in the ALG basin in contrast to the ION and TYR basins where remineralization is mainly located in the upper 500 m horizon. We proposed that the larger and deeper MR rates in the ALG basin would be sustained by an additional particles export event driven by deep convection. The TYR basin (in contrast to the ALG and ION basins) presents the impact of a previous dust event as reflected by our particulate Al water column concentrations. The ION and TYR basins are also the site of small-scale heterogeneity of stages of remineralization processes, as especially reflected by our Ba_{xs} inventories and integrated PHP data at the #Tyr long duration station. This heterogeneity is linked to the mosaic of blooming and non-blooming patches reported in this area during the cruise. Contrastingly to the western Mediterranean Sea (ALG basin), the central Mediterranean Sea (ION and TYR basins) shows lower (intensity) and upper mesopelagic-layer restricted remineralization processes during the late spring PEACETIME cruise.

1. Introduction

In the ocean, remineralization rate associated with sinking particles is a crucial variable for air sea CO_2 balance [Kwon et al., 2009]. Most of the sinking particulate organic carbon (POC) conversion (i.e. remineralization) into CO_2 by heterotrophic organisms (i.e. respiration) occurs within the mesopelagic zone (100-1000 m) [Martin et al., 1987; Buesseler et al., 2007; Buesseler and Boyd, 2009]. A quantitative representation of this process is thus crucial to future predictions of the ocean's role in the global C cycle [IPCC, 2014]. Particulate biogenic barium (Ba_{xs}) is a geochemical tracer of POC remineralization in the mesopelagic layer. Ba_{xs} occurs in the form of barite ($BaSO_4$ crystals) in the dark ocean as a byproduct of prokaryotic remineralization. In a global ocean undersaturated with respect to barite [Monnin and Cividini, 2006], Ba_{xs} precipitates inside oversaturated biogenic micro-environments during POC degradation by heterotrophic prokaryotes, through sulfate and/or barium enrichment [Dehairs et al., 1980; Stroobant et al., 1991; Bertram and Cowen, 1997; Ganeshram et al., 2003]. By applying a transfer function relating Ba_{xs} to O_2 consumption [Dehairs et al., 1997] Ba_{xs} has been widely used since the 90's as an estimator of mesopelagic POC remineralization rates in various sectors of the Southern Ocean, North Pacific and North Atlantic [Cardinal et al., 2001, 2005; Dehairs et al., 2008; Jacquet et al., 2008a, 2008b, 2011, 2015; Planchon et al., 2013; Lemaitre et al., 2018]. Jacquet et al. [2021] recently reported that such transfer function could be applied in the Mediterranean Sea without restriction. This last study complemented previous investigations aiming at improving the use of Ba_{xs} to estimate local processes of POC remineralization in the Mediterranean Sea [Jacquet et al., 2016; Jullion et al., 2017]. The Mediterranean Sea represents a unique case study, mainly due to unresolved issues related to the imbalance in the regional C budget such as the coupling between surface biology and deeper remineralization, timescales of their variability between basins and discrepancies between mesopelagic trophic structure and respiration dynamics

63 [Sternberg et al., 2007, 2008; Santinelli et al., 2010; Lopez-Sandoval et al., 2011; Luna et al.,

64 2012; Tanhua et al., 2013b; Malanotte-Rissoli et al., 2014].

65   The present work is part of the PEACETIME project (ProcEss studies at the Air-sEa

66 Interface after dust deposition in the MEditerranean sea) (http://peacetime-project.org/). It

67 aimed at studying the impact of atmospheric Saharan dust on the Mediterranean

68 biogeochemistry [Guieu et al., 2020a]. Dust deposition is a major source of macro and micro

69 nutrients and ballasted material to surface waters that likely impacts the biological carbon

70 pump through organic matter production (i.e. primary production) and its subsequent export

71 and remineralization in the water column [Pabortsava et al., 2017; Gazeau et al., 2021].

72 Overall, the aims of the present contribution to the PEACTIME project were: (1) to document

73 particulate biogenic Ba_{xs} in different ecoregions of the western and central parts of the

74 Mediterranean Sea. Previous Ba_{xs} data in the Mediterranean Sea are relatively scarce with

75 limited vertical sampling resolution [Sanchez-Vidal et al., 2005] or restricted locations

76 [Dehairs et al., 1987; Sternberg et al., 2007, 2008; van Beek et al., 2009]; (2) to determine the

77 relationship between Ba_{xs} and environmental variability, including dust deposition, (3) to

78 estimate Ba_{xs}-based POC remineralization rates (MR) at mesopelagic depths using the

79 Dehairs' transfer function [Dehairs et al., 1997] which we have recently validated for the

80 Mediterranean Sea [Jacquet et al., 2021], and (4) assess potential differences in

81 remineralization length scale of POC in the various ecoregions of the Mediterranean Sea.

82

83 **2. Material and methods**

84 **2.1 Study area**

85   The PEACETIME cruise (https://doi.org/10.17600/17000300) was conducted during late

86 spring from May 10 to June 11, 2017 (French R/V Pourquoi pas?) in the western and central

87 Mediterranean (Figure 1a). The Mediterranean Sea is a semi-landlocked sea, with limited but

crucial exchange with the Atlantic Ocean, two deep overturning cells, one shallow circulation and a complex upper layer circulation with several permanent and quasi-permanent eddies.

The hydrography during the PEACETIME cruise was characterized by three-layers: surface, intermediate and deep waters, typical for the Mediterranean [Tamburini et al., 2013; Tanhua et al., 2013a; Hainbucher et al., 2014, Malanotte-Rizzoli et al., 2014]. Briefly, the main water masses are (see potential temperature – salinity diagram in Figure 1b): (1) from west to east surface Atlantic Water (SW) is gradually replaced by Ionian surface Water (ISW) and Levantine Surface water (LSW); (2) Winter Intermediate Water (WIW) and Levantine Intermediate water (LIW). LIW is present at intermediate depths (from 200 to 800 m) and is characterized by a local maximum of salinity and a local minimum of dissolved oxygen concentration; (4) Mediterranean Deep Water (MDW).

Three main ecoregions [Reygondeau et al., 2017; Ayata et al., 2018] were crossed during the cruise: the Algero-Provençal basin (later referred to as ALG), the Tyrrhenian basin (TYR) and the Ionian basin (ION) (Figure 1a). These basins displayed the typical eastward oligotrophic gradient as reported in previous studies [Moutin and Raimbault, 2002; Durrieu de madron et al., 2011; Pujo-Pay et al., 2011; Tanhua et al., 2013a; Reygondeau et al., 2017; Guieu et al., 2020a]. However, this trend was not homogeneous, as for instance in the Ionian Sea (a crossroad of waters of contrasted biological history) where a mosaic of blooming and non-blooming areas co-occured in spring [Berline et al., 2021]. A diatom-dominated deep chlorophyll maximum that coincided with a maximum in biomass and primary production (PP) was well developed and observed all along the cruise track (Marañón et al., 2021). PP is described in details in Van Wambeke et al. (this issue). Furthermore, important dust deposition affected the TYR basin a few days before our arrival at stations #Tyr and #5, while in the ALG basin, dust deposition occurred few hours before our sampling at station

112 #Fast (Bressac et al., this issue). POC downward fluxes measured at 200 m depth were similar

113 at the 3 long stations (#Fast, #Tyrr and #Ion).

114

2.2 Barium sampling and sample processing

116   Thirteen stations were sampled for particulate barium from the surface to 2000 m (thirty

117 depths in total) in the ALG (stations #1, #2, #3, #10, #Fast, #9 and #4), TYR (stations #5,

118 Tyrr and #6) and ION (stations #8, #7 and #Ion) basins (Table 1). Three of these stations were

119 sampled twice on different days (long duration stations #Fast, #Tyrr and #Ion), but due to

120 technical problem no particulate barium data are available for the second visit at station #Ion.

121 Three days separate both visits at station #Fast and two days at #Tyrr.

122   For particulate barium, 4 to 6 L of seawater sampled using Niskin bottles were filtered onto

123 47 mm polycarbonate membranes (0.4 μm porosity) under slight overpressure supplied by

124 filtered air. Filters were rinsed with a few mL of MQ grade water to remove sea salt, dried

125 (50°C) and stored in Petri dishes for later analysis. In the laboratory, we performed a total

126 digestion of filters using a concentrated tri-acid (0.5 mL HF /1.5 mL HNO_3 / HCl 1 mL; all

127 Optima grade) mixture in closed teflon beakers overnight at 95°C in a clean pressurized room.

128 After evaporation close to dryness, samples were re-dissolved into 10 mL of 2% HNO_3.

129 Subsequently, samples were analysed for Ba and other elements of interest (i.e. Al, Na, Sr and

130 Ca) by HR-ICP-MS (High Resolution-Inductively Coupled Plasma- Mass Spectrometry;

131 ELEMENT XR, Thermo). Based on analyses of external certified reference standards,

132 accuracy and reproducibility were both within ±5%. More details on sample processing and

133 analysis are given in Cardinal et al. [2001] and Jacquet et al. [2015]. The presence of sea-salt

134 was checked by analysing Na and the sea-salt particulate Ba contribution was found to be

135 negligible (<0.1% of total Ba). Particulate biogenic barium in excess (hereafter referred to as

136 Ba_{xs}) was calculated as the difference between total Ba and lithogenic Ba. The lithogenic Ba

137 concentration was determined using Al concentration and the upper continental crust (UCC)

138 Ba:Al molar ratio [Dymond et al., 1992; Taylor and Mc Lennan, 1985]. The standard

139 uncertainty [Ellison et al., 2000] on Ba_{xs} concentration ranges between 5.0 and 5.5%. The

140 term "in excess" is used to indicate that concentrations are larger than the Ba_{xs} background

141 (Ba BKG). The background (or residual value) is considered as "preformed" Ba_{xs} at zero

142 oxygen consumption left over after transfer and partial dissolution of Ba_{xs} produced during

143 degradation of previous particles export events. This background Ba_{xs} value likely depends on

144 the saturation state of the water with respect to barite ($BaSO_4$, the main phase of particulate

145 biogenic barium). Saturation indexes were reported in Jacquet et al. [2016] over a high

146 resolution and quasi-zonal Mediterranean transect (M84/3 cruise; Tanhua et al., 2013a,

147 2013b). They revealed that the water column throughout the study area is largely

148 undersaturated, with saturation state ranging between 0.2 and 0.6. A background Ba_{xs} value of

149 130 pM was recently reported in Jacquet et al. [2021]. It is close to the average Ba_{xs} contents

150 observed at greater depth (>1000 m) in the present study (see below).

151

2.3 Prokaryotic heterotrophic production

153 Prokaryotic heterotrophic production (PHP) estimation was measured by the L-[4,5-3H]-

154 Leucine (^{3}H-Leu, specific activity 109 Ci mmol^{-1}, PerkinElmer®) incorporation technique

155 (Kirchman, 1993). Details of the protocols can be found in Van Wambeke et al. (2021).

156 Briefly, in epipelagic layers (0-200 m) 1.5 ml seawater samples were incubated at 20 nM ^{3}H-

157 Leu final concentration using the microcentrifuge technique (Smith and Azam, 1992). For the

158 mesopelagic layers, 20 ml (200-800 m depth) and 40 ml (below 800 m depth) seawater

159 samples were incubated using 20 nM and 10 nM ^{3}H-Leu final concentration, respectively,

160 using the filtration technique (Tamburini et al., 2002). Samples were incubated at in situ

161 temperature. To calculate PHP, we used the empirical conversion factor of 1.5 ng C per pmol

162   of incorporated leucine assuming that isotopic dilution was negligible under saturating

163   concentrations of leucine as checked occasionally from concentration kinetics (Van Wambeke

164   et al., 2021).

165

166   **2.4 POC remineralization rates**

167   We recently reported on the validity of the Dehairs's transfer function [Dehairs et al., 1997]

168   in the Mediterranean basin to estimate mesopelagic POC remineralization [Jacquet et al.,

169   2021]. We applied the similar approach to estimate remineralization rates (MR):

170     $MR = [(Ba_{xs} - Ba\ BKG)/17450] \times Z \times RR$ (Eq.1)

171   where Ba_{xs} is the depth-weighted average Ba_{xs} concentration (DWA; pM), i.e. the Ba_{xs}

172   inventory divided by the depth layer considered Z, and RR the Redfield C/O_2 molar ratio

173   (127/175; Broecker et al., 1985). As reported above, a Ba BKG concentration of 130 pM was

174   used. MR rates were then integrated over the 100-500 m (upper mesopelagic zone) and 100-

175   1000 m (entire mesopelagic zone) depth layers.

176

177   **3. Results**

178   Particulate biogenic Ba_{xs}, biogenic Ba fraction (%) and particulate Al, Sr and Ca

179   concentrations are reported in Figure 2 in the upper 2000 m of the water column along a zonal

180   transect crossing the three main sub-basins. PHP rates are also reported in Figure 2 in the

181   upper 500 m along the same transect.

182   Ba_{xs} displayed a similar water column distribution as reported in various sectors of the

183   global Ocean, i.e. relatively low surface concentrations, a maximum in the mesopelagic layer

184   (100-1000 m) followed by a decrease of concentrations back to a background level at deeper

185   depths, usually 1000 m (Figure 3). At stations #9, #Tyrr, #8 and #Ion, Ba_{xs} concentrations in

186   the upper 100 m were quite high (>5000 pM), with values reaching up to 11700 pM at 80 m

187   depth at station #Tyrr (Figure 2a). Such high Ba_{xs} concentrations in the upper layers are quite

188   unusual, though similar values (up to 9000 pM) were occasionally observed in earlier

189   Southern Ocean studies [Dehairs et al., 1991, 1997; Jacquet et al., 2007b, 2008a, 2008b]. The

190   high Ba_{xs} values at stations #Tyrr and #Ion were associated with higher Sr (up to 4267 pM at

191   100 m at station #Ion) and Ca (>130 nM) concentrations (Figure 2d, e). Thoughtout the water

192   column, Sr and Ca concentrations ranged from to 448 to 6938 pM and from 30 to 488 nM,

193   respectively. Sr/Ca molar ratios ranged from 7 to 45 mmol mol^{-1}whithin the range of ratios

194   reported in organic material [Martin and Knauer, 1976]. The upper mesopelagic layer (100-

195   500 m) showed the characteristic Ba excess (maximum), as illustrated in Figure 3a. The

196   lithogenic impact on the Ba_{xs} signal was relatively low (<20 %) except at stations #4, #5 and

197   #Tyrr where it reached up to 30 % at some depths in the water column (Figures 2b, 3b). High

198   Ba_{xs} concentrations at stations in the ALG basin and at station #7 in the ION basin extended

199   deeper than at stations in the TYR basin (Figure 2a). At station #Ion Ba_{xs} maximum coincided

200   with higher Ca (up to 186 nM) concentrations in the upper mesopelagic layer (Figure 2e).

201   However, the Ba_{xs} maximum also extented deeper. This is especially salient at stations in the

202   ALG basin. At the other stations Ba_{xs} concentrations below 500 m decreased to reach the

203   background value of around 130 pM. Among stations sampled twice for barium during the

204   cruise, station #Fast (ALG basin) presented similar Ba_{xs} profiles except between 400 and

205   1000 m depth where lower concentrations were measured during the second visit (3 days

206   later; Figure 3a). The Ba_{xs} signal was mostly biogenic and rather stable over the whole water

207   column at this station. This was also the case at station #Ion. In contrast, at station #Tyrr

208   differences between Ba_{xs} profiles mainly occurred in the surface layer and upper mesopelagic

209   layer, with relatively higher Ba_{xs} peaks during the second visit (2 days later; Figure 3b). The

210   biogenic Ba fraction was also more variable throughout the water column at #Tyrr.

211   PHP rates decreased from west to east in surface waters (Figure 2f). At station #Fast,

212   PHP rates decreased from 49 ng C l^{-1} h^{-1} in surface to values between 7 and 11 ng C l^{-1} h^{-1} at

213   100 m depth and below 6 ng C l^{-1} h^{-1} below 200 m depth (Figure 3d). Same trends were found

214   at #Tyrr and #Ion with values in surface waters around 36 and 25 ng C l^{-1} h^{-1} respectively

215   (Figures 3e and 3f).

216   Depth-weighted average (DWA) concentrations of Ba_{xs} are reported in Table 1 and

217   Figure 5 for the upper (100-500 m) and entire (100-1000 m) mesopelagic layer. Since the base

218   of the mixed layer was shallower than 100 m, this depth is taken as the upper boundary of the

219   mesopelagic domain. DWA values ranged from 221 to 979 pM. On average, stations located

220   in the ALG basin presented higher DWA than in the TYR and ION basins. DWA Ba_{xs} values

221   remained rather stable over the 3–day period at station #Fast between 100 and 500 m depth,

222   but decreased in deeper layers (Figure 5). As a consequence, the DWA changed from 527 to

223   381 pM for the entire 100-1000 depth layer. In contrast, at station #Tyrr DWA Ba_{xs} values for

224   the 100-500 m and 100-1000 m depth layers increased over the 2–day period (from 284 to

225   542 pM and from 200 to 380 pM, respectively). On average DWA Ba_{xs} reached 577±286,

226   378±123 and 529±213 pM (100-500 m), and 527±288, 280±82 and 358±112 pM (100-1000

227   m) in the ALG, TYR and ION basin, respectively.

228

229   **4. Discussion**

230   **4.1 Ba_{xs} distributions across the sub-basins**

231   The very high Ba_{xs} concentrations reported in the surface layer at stations #9, #Tyrr,

232   #8 and #Ion were associated with local Sr and Ca maxima, likely linked to potentially

233   ballasted phytoplankton-derived material. Similar observations were previously reported in

234   the Southern Ocean, revealing that in the surface water particulate Ba_{xs} is incorporated into or

235   adsorbed onto biogenic material, with barite being a minor component [Dehairs et al., 1991,

236   1997; Jacquet et al., 2007a, 2008a, 2008b]. In deeper layers, Ba_{xs} presented the characteristic

maximum reflecting mesopelagic remineralization processes. Mesopelagic Ba_{xs} distributions presented here were similar to those reported in Jacquet et al. [2021] and Sternberg et al. [2008] in the northwestern Mediterranean Sea (ANTARES and DYFAMED observatory sites, respectively). The Ba_{xs} maximum extended down to 1000 m depth in the ALG basin, while it was mostly located in the upper 500 m depth in the TYR basin. The lithogenic impact on the Ba_{xs} signal was relatively very low (<5%), except at stations #4, #5 and #Tyrr where it was more variable and reached up to 30 % at some depths (Figure 2b and 2c). A large dust deposition event occurred over a large area including the southern Tyrrhenian Sea just before the beginning of the PEACETIME campaign. Particulate Al concentrations and estimated lithogenic Ba fraction were sampled at these stations 5 to 12 days after the event and reflected the impact of this dust event in depth. These conclusions are further supported by results reported in Bressac et al. [this issue], showing that Saharan dust depositions strongly impacted Stations #4, #5, #Tyr and #6 whereby a significant fraction of dust particles was transferred to mesopelagic depths.

4.2 Mesopelagic Ba_{xs} and prokaryotic heterotrophic production

Previous studies highlighted the relationship between the mesopelagic Ba_{xs} and the vertical distribution of prokaryotic heterotrophic production (PHP), reflecting the temporal progression of POC remineralization processes. In mesopelagic layers, Ba_{xs} content is smaller when most of the PHP occurs in the upper mixed layer (indicating an efficient, close to complete remineralization within the surface), compared to situations where a significant part of PHP is located deeper in the water column (reflecting significant deep prokaryotic activity and POC export). Figure 3 shows the PHP profiles at long station #Fast, #Tyr and #Ion (see also VanWambeke et al. [2021] for more detail on PHP). Figure 4 shows the ratio of integrated surface (100 m) to integrated upper mesopelagic (500 m) PHP vs. DWA Ba_{xs}

262 calculated over the 100-500 m depth interval. Results are confronted to the data obtained in

263 the Southern Ocean [Jacquet et al., 2008a, 20015] and recently in the northeast Atlantic and

264 northwestern Mediterranean Sea (PAP and ANTARES observatory sites, respectively)

265 [Jacquet et al., 2021]. The blue line in Figure 4 represents the trend obtained during KEOPS2

266 [Jacquet et al., 2015]; it does not include encircled data points referred to as "season

267 advancement". Results during PEACETIME followed a similar trend than found for KEOPS2

268 with higher DWA Ba_{xs} in situation where a significant part of column-integrated PHP is

269 located deeper in the water column (high Int.PHP100/Int.PHP500 ratio, Figure 4). Note that

270 some data points, characterized by low DWA Ba_{xs} values, did not follow the trend from

271 KEOPS2 (stations #3, #5 and #Tyrr2). During KEOPS2, the lowest DWA were reported for

272 stations located in a meander and reflecting different (earlier) stages of a bloom compared to

273 the other stations (see "season advancement" in Figure 4). Similarly, station #5 and #Tyrr2

274 reflected the temporal evolution of the establishment (or advanced stages) of mesopelagic

275 remineralization processes in the TYR basin compared to the other basins. Measurements

276 carried out during the second visit at station #Tyrr two days later corroborated this hypothesis

277 showing an increase in remineralization in the upper mesopelagic layer (DWV Ba_{xs} increased

278 from 284 to 542 pM). At the DYFAMED station, Sternberg et al. [2008] reported the seasonal

279 evolution of Ba_{xs} profiles on a monthly basis between February and June 2003. These authors

280 showed the mesopelagic Ba_{xs} build up (and barite stock increase) following the spring

281 phytoplankton bloom development, enhanced POC fluxes and subsequent remineralization.

282 Overall, DWA Ba_{xs} reported in the present study were higher than those reported by

283 Sternberg et al. [2008] (maximum of 463 pM; 0-600 m). The variability over the two days

284 period at station #Tyrr was of the same order of magnitude as the seasonal DWA Ba_{xs}

285 dynamics found at DYFAMED and similar to changes found over a few days to week period

286 in different sectors of the Southern Ocean [Cardinal et al., 2005; Jacquet et al., 2007a; 2015].

287   The column-integrated PHP vs. DWA Ba_{xs} ratio at station #Tyrr confirms that the second

288   occupation experienced higher remineralization rates in the upper mesopelagic layer than

289   during the first one (Table 1).

290

291   **4.3 Mesopelagic C remineralization**

292   POC remineralization rates (MR) estimated from DWA Ba_{xs} values using Eq. (1) are shown

293   in Figure 5 for the upper (100-500 m) and entire (100-1000 m) mesopelagic layer together

294   with primary productivity [van Wambecke et al., 2021]. MR ranged from 25 ± 2 to 306 ± 70

295   mg C m^{-2} d^{-1} and primary production ranged from 138 to 284 mg C m^{-2} d^{-1}. Large difference

296   in MR between the upper and the whole mesopelagic layers can be seen in the ALG basin.

297   This is more pronounced at station #9 with MR of 91 mg C m^{-2} d^{-1} in the upper (100 to 500 m

298   depth) layer and 306 mg C m^{-2} d^{-1} in the entire mesopelagic layer (Figure 5). These results

299   show that significant remineralization occurred between 500 and 1000 m in the ALG basin in

300   contrast to the ION and TYR basins where remineralization occurred mainly in the

301   mesopelagic layer between 100 and 500 m depth. Similar conclusion was reached by Jullion

302   et al. [2017] from dissolved Ba and Parametric Optimum Multiparameter (POMP)-derived

303   POC remineralization rates along a zonal transect between the Lebanon coast and Gibraltar

304   (from 156 to 348 mg C m^{-2} d^{-1}; M84/3 cruise, April 2011). Independent of any dust input

305   considerations, Jullion et al. [2017] showed significant differences in the mesopelagic MR

306   between the western and eastern Mediterranean, indicating an additional organic carbon

307   export pathway to depth. The western basin is indeed the site of deep shelf and open ocean

308   convection, transferring organic matter to deeper layers [Durrieu de Madron et al., 2013;

309   Stabholz et al., 2013]. The larger MR fluxes found in the ALG basin during PEACETIME are

310   in line with an ecoregion with recurrent injection of material by winter convection (hypothesis

311   of particle injection pump; Boyd et al. [2019]), sustaining higher rates of remineralization

below 500 m depth. In contrast in the TYR basin remineralization was mainly located in the upper mesopelagic layer. Stations in the TYR basin received dust inputs a few days before our arrival at these stations; the particulate Al concentrations and estimated lithogenic Ba fraction reflected the impact of this event (Figure 2; Bressac et al., this issue). At station #Tyrr the DAW Ba_{xs} vs. column-integrated PHP increase between the two visits indicated higher MR rates. MR were mainly localized in the upper 500 m. Another atmospheric deposition event occurred on June 5, a few hours after the first sampling at station #Fast in the ALG basin. However, station #Fast does not present any evidence of an impact at mesopelagic depths on particulate Al concentrations and estimated lithogenic Ba. In contrast to conditions in the surface mixed layer, the generation of an observable signal from the mesopelagic remineralization and subsequent Ba_{xs} formation to a single dust event would require more time than the time span between atmospheric deposition and sampling at #Fast (in contrast to station #Tyrr where the dust event occurred 5 to 12 days before). In the ION basin where stations did not reflect the impact of any deposition event and were not subject to potential deep convection, DWA Ba_{xs} and MR fluxes were mostly restricted to the upper mesopelagic layer. Berline et al. [this issue] report small-scale heterogeneity of particles abundances at ION stations, emphasizing the spatial decoupling between particle production and particle distribution and adding complexity in estimating the time lag between production and export of particles, and thus C transfer eat depth [Stange et al., 2017; Henson et al., 2011]. Further, no significant surface production event occurred in the ION basin However, surface particles at station #8 seemed related to a past production event without significant vertical export by the time the station was sampled. As reported in Van Wambeke et al. [this issue], primary production fluxes were slightly higher in the ION basin (from 158 to 208 mg C m^{-2} d^{-1}) than in the TYR basin (from 142 to 170 mg C m^{-2} d^{-1}). Overall, DWA Ba_{xs} and MR fluxes reported in the ION basin would thus reflect earlier stage of export and remineralization processes. The

337 same applies to station #Tyrr 2 (in contrast to #Tyrr4) according to the DWA Ba_{xs} vs

338 integrated-PHP trend.

339

5. Conclusion

341 The present paper expands the data coverage of Ba_{xs} distribution in the ALG, TYR and

342 ION basins (western and central Mediterranean Sea) in late spring 2017. Results highlight that

343 mesopelagic remineralization processes are mainly located in the upper 500 m horizon in the

344 TYR and ION basins, while they occur in the lower mesopelagic zone (down to 1000 m) in

345 the ALG basin. We suggest that particle injection driven by the seasonal winter deep

346 convection in the western basin would sustain the larger and deeper MR rates we observed in

347 the ALG basin. At both TYR and ION basins, Ba_{xs} indicated lower (intensity) and upper

348 mesopelagic-layer restricted remineralization processes that could be the results of a previous

349 dust deposition event (in particular at #Tyr) or the patchiness of time lags between

350 production and export of particles.

351

Data availability

353 Underlying research data are being used by researcher participants of the PEACETIME

354 campaign to prepare other papers, and therefore data are not publicly accessible at the time of

355 publication. Data will be accessible once the special issue is completed (June 2021)

356 (http://www.obs-vlfr.fr/proof/php/PEACETIME/peacetime.php; last access 02/04/2021). The

357 policy of the database is detailed here: http://www.obs-vlfr.fr/proof/dataconvention.php and

358 https://www.seanoe.org/data/00645/75747/ (last access 02/04/2021).

359

Author contributions

361 SJ wrote the manuscript with the contribution of all co-authors.

362

Competing interests

The authors declare that they have no known competing financial interests or personal relationships that could have appeared to influence the work reported in this paper.

Special issue statement

This article is part of the special issue "Atmospheric deposition in the low-nutrient–low-chlorophyll (LNLC) ocean: effects on marine life today and in the future (ACP/BG interjournal SI)". It is not associated with a conference.

Acknowledgments

This study is a contribution to the PEACETIME project (http://peacetime-project.org), a joint initiative of the MERMEX and ChArMEx components supported by CNRS-INSU, IFREMER, CEA, and Météo-France as part of the programme MISTRALS coordinated by INSU. PEACETIME was endorsed as a process study by GEOTRACES. It is also a contribution to SOLAS and IMBER. We thank the captain and the crew of the RV Pourquoi Pas? for their professionalism and their work at sea. We warmly thank C. Guieu and K. Deboeufs, as coordinators of the program PEACETIME and chiefs scientists of the campaing. This work is a contribution to the "AT – POMPE BIOLOGIQUE" of the Mediterranean Institute of Oceanography (MIO). The instrument (ELEMENT XR, ThermoFisher) was supported in 2012 by European Regional Development Fund (ERDF).

Figures

Figure 1: (a) Map of the study area showing the three sub-basins (ALG, TYRR and ION) with stations' locations. The dashed line represents the zonal transect reported in Figure 2; (b) Potential temperature – salinity diagram with isopynals (kg m^{-3}) for PEACETIME profiles. Graph produced using Ocean Data View (Schlitzer, 2002).

Figure 2: Sections of (a) particulate biogenic Ba (Ba$_{xs}$, pM), (c) Al (pM), (d) Sr (pM) and (e) Ca (nM) concentrations, and (b) % biogenic Ba (Ba$_{xs}$) in the upper 2000 m water column. (f) Section of PHP (ngC L^{-1} h^{-1}) in the upper 500 m of the water column. Graph produced using Ocean Data View (Schlitzer, 2002).

Figure 3: (a-c) Ba$_{xs}$ (pM) and (d-f) (ngC L^{-1} h^{-1}) profiles in the upper 2000 m and 1000 m of the water column, respectively, at long stations #Fast, #Tyrr and #Ion. (a-c) The dashed grey line represents the Ba$_{xs}$ background (BKG) and the grey area represents the fraction for which Ba$_{xs}$ is mostly biogenic.

Figure 4: Ratio of surface layer integrated PHP (Int.PHPx1) to mesopelagic integrated PHP (Int.PHPx2) versus mesopelagic depth-weighted average (DWA) Ba$_{xs}$ (pM) during PEACETIME. The same data are reported for the KEOPS1 and KEOPS2 cruises (Southern Ocean; Jacquet et al., 2015) and at the PAP (NE-Atlantic) and ANTARES/EMSO-LO (NW-Mediterranean Sea) observatory sites (Jacquet et al., 2021). The blue line (R^2=0.88) represents the trend reported during KEOPS2 (Jacquet et al., 2005). The data points referred to as "season advancement" (encircle by the blue line) were excluded from the KEOPS2 regression analysis shown here.

408

409 Figure 5: integrated POC remineralization rates (mg C m^{-2} d^{-1}) in the upper (100 to 500 m

410 depth) and entire (100 to1000 m depth) mesopelagic layer in the ALG, TYR and ION basins.

411 Open squares represent primary production (mg C m^{-2} d^{-1}; Van Wambeke et al., this issue).

412

413

414 **Tables**

415 Table 1: Depth-weighted average (DWA) concentrations of Ba_{xs} (pM) and remineralization

416 rates (MR; mg C m^{-2} d^{-1}) for the upper (100 to 500 m depth) and entire (100 to 1000 m depth)

417 mesopelagic layer.

418 **References**

419 Ayata, S.-D., Irisson, J.-O., Aubert, A., Berline, L., Dutay, J.-C., Mayot, N., Nieblas, A.-E.,

420 D'Ortenzio, F., Palmiéri, J., Reygondeau, G., Rossi, V., and Guieu, C.: Regionalisation of the

421 Mediterranean basin, a MERMEX synthesis, Prog. Oceanogr., 163, 7–20,

422 https://doi.org/10.1016/j.pocean.2017.09.016, 2018.

423 van Beek, P., Sternberg, E., Reyss, J.-L., Souhaut, M., Robin, E., and Jeandel, C.:

424 228Ra/226Ra and 226Ra/Ba ratios in the Western Mediterranean Sea: Barite formation and

425 transport in the water column, Geochim. Cosmochim. Ac., 73, 4720–4737,

426 https://doi.org/10.1016/j.gca.2009.05.063, 2009.

427 Berline, L., Doglioli, A. M., Petrenko, A., Barrillon, S., Espinasse, B., Le Moigne, F. A. C.,

428 Simon-Bot, F., Thyssen, M., and Carlotti, F.: Long distance particle transport to the central

429 Ionian Sea, Biogeosciences, 2021, 1–28, https://doi.org/10.5194/bg-2020-481, 2021.

430 Bertram, M. and P. Cowen, J.: Morphological and compositional evidence for biotic

431 precipitation of marine barite, J. Mar. Res., 55, 577–593, 1997.

432 Boyd, P., Claustre, H., Levy, M., Siegel, D., and Weber, T.: Multi-faceted particle pumps

433 drive carbon sequestration in the ocean, Nature, 568, 327–335,

434 https://doi.org/10.1038/s41586-019-1098-2, 2019.

435 Broecker, W. S., Takahashi, T., and Takahashi, T.: Sources and flow patterns of deep-ocean

436 waters as deduced from potential temperature, salinity, and initial phosphate concentration, J.

437 Geophys. Res., 90, 6925–6939, https://doi.org/10.1029/JC090iC04p06925, 1985.

438 Buesseler, K. O. and Boyd, P. W.: Shedding light on processes that control particle export and

439 flux attenuation in the twilight zone of the open ocean, Limnol. Oceanogr., 54, 1210–1232,

440 https://doi.org/10.4319/lo.2009.54.4.1210, 2009.

441 Buesseler, K. O., Lamborg, C. H., Boyd, P. W., Lam, P. J., Trull, T. W., Bidigare, R. R.,

442 Bishop, J. K. B., Casciotti, K. L., Dehairs, F., Elskens, M., Honda, M., Karl, D. M., Siegel, D.

A., Silver, M. W., Steinberg, D. K., Valdes, J., Van Mooy, B., and Wilson, S.: Revisiting Carbon Flux Through the Ocean's Twilight Zone, Science, 316, 567–570, https://doi.org/10.1126/science.1137959, 2007.

Cardinal, D., Dehairs, F., Cattaldo, T., and André, L.: Geochemistry of suspended particles in the Subantarctic and Polar Frontal zones south of Australia: Constraints on export and advection processes, J. Geophys. Res., 106, 31637–31656, https://doi.org/10.1029/2000JC000251, 2001.

Cardinal, D., Savoye, N., Trull, T. W., André, L., Kopczynska, E. E., and Dehairs, F.: Variations of carbon remineralisation in the Southern Ocean illustrated by the Baxs proxy, Deep-Sea Res. Pt. I, 52, 355–370, https://doi.org/10.1016/j.dsr.2004.10.002, 2005.

Dehairs, F., Chesselet, R., and Jedwab, J.: Discrete suspended particles of barite and the barium cycle in the open ocean, Earth. Planet. Sc. Lett., 49, 528–550, https://doi.org/10.1016/0012-821X(80)90094-1, 1980.

Dehairs, F., Lambert, C. E., Chesselet, R., and Risler, N.: The biological production of marine suspended barite and the barium cycle in the Western Mediterranean Sea, Biogeochemistry, 4, 119–140, https://doi.org/10.1007/BF02180151, 1987.

Dehairs, F., Stroobants, N., and Goeyens, L.: Suspended barite as a tracer of biological activity in the Southern Ocean, Mar. Chem., 35, 399–410, http://dx.doi.org/10.1016/S0304-4203(09)90032-9, 1991.

Dehairs, F., Shopova, D., Ober, S., Veth, C., and Goeyens, L.: Particulate barium stocks and oxygen consumption in the Southern Ocean mesopelagic water column during spring and early summer: relationship with export production, Deep-Sea Res. Pt. II, 44, 497–516, https://doi.org/10.1016/S0967-0645(96)00072-0, 1997.

Dehairs, F., Jacquet, S., Savoye, N., Van Mooy, B. A. S., Buesseler, K. O., Bishop, J. K. B., Lamborg, C. H., Elskens, M., Baeyens, W., Boyd, P. W., Casciotti, K. L., and Monnin, C.:

468 Barium in twilight zone suspended matter as a potential proxy for particulate organic carbon

469 remineralization: Results for the North Pacific, Deep-Sea Res. Pt. II, 55, 1673–1683,

470 https://doi.org/10.1016/j.dsr2.2008.04.020, 2008.

471 Durrieu de Madron, X., Guieu, C., Sempéré, R., Conan, P., Cossa, D., D'Ortenzio, F.,

472 Estournel, C., Gazeau, F., Rabouille, C., Stemmann, L., Bonnet, S., Diaz, F., Koubbi, P.,

473 Radakovitch, O., Babin, M., Baklouti, M., Bancon-Montigny, C., Belviso, S., Bensoussan, N.,

474 Bonsang, B., Bouloubassi, I., Brunet, C., Cadiou, J.-F., Carlotti, F., Chami, M., Charmasson,

475 S., Charrière, B., Dachs, J., Doxaran, D., Dutay, J.-C., Elbaz-Poulichet, F., Eléaume, M.,

476 Eyrolles, F., Fernandez, C., Fowler, S., Francour, P., Gaertner, J. C., Galzin, R., Gasparini, S.,

477 Ghiglione, J.-F., Gonzalez, J.-L., Goyet, C., Guidi, L., Guizien, K., Heimbürger, L.-E.,

478 Jacquet, S. H. M., Jeffrey, W. H., Joux, F., Le Hir, P., Leblanc, K., Lefèvre, D., Lejeusne, C.,

479 Lemé, R., Loÿe-Pilot, M.-D., Mallet, M., Méjanelle, L., Mélin, F., Mellon, C., Mérigot, B.,

480 Merle, P.-L., Migon, C., Miller, W. L., Mortier, L., Mostajir, B., Mousseau, L., Moutin, T.,

481 Para, J., Pérez, T., Petrenko, A., Poggiale, J.-C., Prieur, L., Pujo-Pay, M., Pulido-Villena,

482 Raimbault, P., Rees, A. P., Ridame, C., Rontani, J.-F., Ruiz Pino, D., Sicre, M. A.,

483 Taillandier, V., Tamburini, C., Tanaka, T., Taupier-Letage, I., Tedetti, M., Testor, P.,

484 Thébault, H., Thouvenin, B., Touratier, F., Tronczynski, J., Ulses, C., Van Wambeke, F.,

485 Vantrepotte, V., Vaz, S., and Verney, R.: Marine ecosystems' responses to climatic and

486 anthropogenic forcings in the Mediterranean, Prog. Oceanogr., 91, 97–166,

487 https://doi.org/10.1016/j.pocean.2011.02.003, 2011.

488 Dymond, J. R., Suess, E., and Lyle, M.: Barium in deep-sea sediment: a geochemical proxy

489 for paleoproductivity, Paleoceanography, 7, 163–181, 1992.

490 Ellison, S. L. R.: Eurachem/CITAC Guide CG4, Quantifying Uncertainty in Analytical

491 Measurement, 2nd Edn., edited by: Ellison, S. L. R., Rosslein, M., and Williams, A., 120 pp.,

492 ISBN 0948926 15 5, 2000.

493   Ganeshram, R. S., François, R., Commeau, J., and Brown-Leger, S. L.: An experimental

494   investigation of barite formation in seawater, Geochim. Cosmochim. Ac., 67, 2599–2605,

495   https://doi.org/10.1016/S0016-7037(03)00164-9, 2003.

496   Gazeau, F., Van Wambeke, F., Marañon, E., Pérez-Lorenzo, M., Alliouane, S., Stolpe, C.,

497   Blasco, T., Leblond, N., Zäncker B., Engel A., Marie, B., Dinasquet, J., and Guieu C.: Impact

498   of dust addition on the metabolism of Mediterranean plankton communities and carbon export

499   under present and future conditions of pH and temperature, Biogeosciences Discuss.

500   [preprint], https://doi.org/10.5194/bg-2021-20, in review, 2021.

501   Guieu, C., D'Ortenzio, F., Dulac, F., Taillandier, V., Doglioli, A., Petrenko, A., Barrillon, S.,

502   Mallet, M., Nabat, P., and Desboeufs, K.: Introduction: Process studies at the air–sea interface

503   after atmospheric deposition in the Mediterranean Sea – objectives and strategy of the

504   PEACETIME oceanographic campaign (May–June 2017), Biogeosciences, 17, 5563–5585,

505   https://doi.org/10.5194/bg-17-5563-2020, 2020a.

506   Guieu, C., and Desboeufs, K. : PEACETIME cruise, RV Pourquoi pas?,

507   https://doi.org/10.17600/17000300, 2017.

508   Guieu, C., Desboeufs, K., Albani, S., et al.: Biogeochemical dataset collected during the

509   PEACETIME cruise, available at: https://www.seanoe.org/data/00645/75747/, 2020b.

510   Hainbucher, D., Rubino, A., Cardin, V., Tanhua, T., Schroeder, K., and Bensi, M.:

511   Hydrographic situation during cruise M84/3 and P414 (spring 2011) in the Mediterranean

512   Sea, Ocean Sci., 10, 669–682, https://doi.org/10.5194/os-10-669-2014, 2014.

513   Henson, S. A., Sanders, R., Madsen, E., Morris, P. J., Le Moigne, F., and Quartly, G. D.: A

514   reduced estimate of the strength of the ocean's biological carbon pump, Geophys. Res. Lett.,

515   38, L04606, https://doi.org/10.1029/2011GL046735, 2011.

516   IPCC: 5th Assessment Report (AR5) Climate Change 2013, Working Group 1, January 2014.

517   Jacquet, S. H. M., Dehairs, F., Elskens, M., Savoye, N., and Cardinal, D.: Barium cycling

518   along WOCE SR3 line in the Southern Ocean, Mar. Chem., 106, 33–45,

519   https://doi.org/10.1016/j.marchem.2006.06.007, 2007a.

520   Jacquet, S. H. M., Henjes, J., Dehairs, F., Worobiec, A., Savoye, N., and Cardinal, D.:

521   Particulate Ba-barite and acantharians in the Southern Ocean during the European Iron

522   Fertilization Experiment (EIFEX), J. Geophys. Res., 112,

523   https://doi.org/10.1029/2006JG000394, 2007b.

524   Jacquet, S. H. M., Savoye, N., Dehairs, F., Strass, V. H., and Cardinal, D.: Mesopelagic

525   carbon remineralization during the European Iron Fertilization Experiment, Global

526   Biogeochem. Cycles, 22, GB1023, https://doi.org/10.1029/2006GB002902, 2008a.

527   Jacquet, S. H. M., Dehairs, F., Savoye, N., Obernosterer, I., Christaki, U., Monnin, C., and

528   Cardinal, D.: Mesopelagic organic carbon remineralization in the Kerguelen Plateau region

529   tracked by biogenic particulate Ba, Deep-Sea Res. Pt. II, 55, 868–879,

530   https://doi.org/10.1016/j.dsr2.2007.12.038, 2008b.

531   Jacquet, S. H. M., Dehairs, F., Dumont, I., Becquevort, S., Cavagna, A.-J., and Cardinal, D.:

532   Twilight zone organic carbon remineralization in the Polar Front Zone and Subantarctic Zone

533   south of Tasmania, Deep-Sea Res. Pt. II, 58, 2222–2234,

534   https://doi.org/10.1016/j.dsr2.2011.05.029, 2011.

535   Jacquet, S. H. M., Dehairs, F., Lefèvre, D., Cavagna, A. J., Planchon, F., Christaki, U.,

536   Monin, L., André, L., Closset, I., and Cardinal, D.: Early spring mesopelagic carbon

537   remineralization and transfer efficiency in the naturally iron-fertilized Kerguelen area,

538   Biogeosciences, 12, 1713–1731, https://doi.org/10.5194/bg-12-1713-2015, 2015.

539   Jacquet, S. H. M., Monnin, C., Riou, V., Jullion, L., and Tanhua, T.: A high resolution and

540   quasi-zonal transect of dissolved Ba in the Mediterranean Sea, Mar. Chem., 178, 1–7,

541   https://doi.org/10.1016/j.marchem.2015.12.001, 2016.

542 Jacquet, S. H. M., Lefèvre, D., Tamburini, C., Garel, M., Le Moigne, F. A. C., Bhairy, N., and

543 Guasco, S.: On the barium–oxygen consumption relationship in the Mediterranean Sea:

544 implications for mesopelagic marine snow remineralization, Biogeosciences, 18, 2205–2212,

545 https://doi.org/10.5194/bg-18-2205-2021, 2021.

546 Jullion, L., Jacquet, S. H. M., and Tanhua, T.: Untangling biogeochemical processes from the

547 impact of ocean circulation: First insight on the Mediterranean dissolved barium dynamics,

548 Global Biogeochem. Cycles, 31, 1256–1270, https://doi.org/10.1002/2016GB005489, 2017.

549 Kirchman, D. L.: Leucine incorporation as a measure of biomass production by heterotrophic

550 bacteria, in: Handbooks of methods in aquatic microbial ecology,, edited by: Kemp, P. F.,

551 Sherr, B. F., Sherr, E. B., and Cole, J. J., Lewis Publishers, Boca Raton, Ann Arbor, London,

552 Tokyo, 509–512, 1993.

553 Kwon, E. Y., Primeau, F., and Sarmiento, J. L.: The impact of remineralization depth on the

554 air–sea carbon balance, Nat. Geosci., 2, 630–635, https://doi.org/10.1038/ngeo612, 2009.

555 Lemaitre, N., Planquette, H., Planchon, F., Sarthou, G., Jacquet, S., García-Ibáñez, M. I.,

556 Gourain, A., Cheize, M., Monin, L., André, L., Laha, P., Terryn, H., and Dehairs, F.:

557 Particulate barium tracing of significant mesopelagic carbon remineralisation in the North

558 Atlantic, Biogeosciences, 15, 2289–2307, https://doi.org/10.5194/bg-15-2289-2018, 2018.

559 López-Sandoval, D. C., Fernández, A., and Marañón, E.: Dissolved and particulate primary

560 production along a longitudinal gradient in the Mediterranean Sea, Biogeosciences, 8, 815–

561 825, https://doi.org/10.5194/bg-8-815-2011, 2011.

562 Luna, G. M., Bianchelli, S., Decembrini, F., De Domenico, E., Danovaro, R., and Dell'Anno,

563 A.: The dark portion of the Mediterranean Sea is a bioreactor of organic matter cycling,

564 Global Biogeochem. Cycles, 26, GB2017, https://doi.org/10.1029/2011GB004168, 2012.

565 Malanotte-Rizzoli, P., Artale, V., Borzelli-Eusebi, G. L., Brenner, S., Crise, A., Gacic, M.,

566 Kress, N., Marullo, S., Ribera d'Alcalà, M., Sofianos, S., Tanhua, T., Theocharis, A., Alvarez,

M., Ashkenazy, Y., Bergamasco, A., Cardin, V., Carniel, S., Civitarese, G., D'Ortenzio, F., Font, J., Garcia-Ladona, E., Garcia-Lafuente, J. M., Gogou, A., Gregoire, M., Hainbucher, D., Kontoyannis, H., Kovacevic, V., Kraskapoulou, E., Kroskos, G., Incarbona, A., Mazzocchi, M. G., Orlic, M., Ozsoy, E., Pascual, A., Poulain, P.-M., Roether, W., Rubino, A., Schroeder, K., Siokou-Frangou, J., Souvermezoglou, E., Sprovieri, M., Tintoré, J., and Triantafyllou, G.: Physical forcing and physical/biochemical variability of the Mediterranean Sea: a review of unresolved issues and directions for future research, Ocean Sci., 10, 281–322, https://doi.org/10.5194/os-10-281-2014, 2014.

Martin, J. H., and G. A. Knauer (1973), Elemental composition of plankton, Geochim. Cosmochim. Acta, 37(7), 1639– 1653.

Martin, J. H., Knauer, G. A., Karl, D. M., and Broenkow, W. W.: VERTEX: carbon cycling in the northeast Pacific, Deep-Sea Res., 34, 267–285, http://dx.doi.org/10.1016/0198-0149(87)90086-0, 1987.

Monnin, C. and Cividini, D.: The saturation state of the world's ocean with respect to (Ba,Sr)SO4 solid solutions, Geochim. Cosmochim. Ac., 70, 3290–3298, https://doi.org/10.1016/j.gca.2006.04.002, 2006.

Moutin, T. and Raimbault, P.: Primary production, carbon export and nutrients availability in western and eastern Mediterranean Sea in early summer 1996 (MINOS cruise), J. Marine Syst., 33–34, 273–288, https://doi.org/10.1016/S0924-7963(02)00062-3, 2002.

Pabortsava, K., Lampitt, R. S., Benson, J., Crowe, C., McLachlan, R., Le Moigne, F. A. C., Mark Moore, C., Pebody, C., Provost, P., Rees, A. P., Tilstone, G. H., and Woodward, E. M. S.: Carbon sequestration in the deep Atlantic enhanced by Saharan dust, Nature Geoscience, 10, 189–194, https://doi.org/10.1038/ngeo2899, 2017.

Planchon, F., Cavagna, A.-J., Cardinal, D., André, L., and Dehairs, F.: Late summer particulate organic carbon export and twilight zone remineralisation in the Atlantic sector of

592   the Southern Ocean, Biogeosciences, 10, 803–820, https://doi.org/10.5194/bg-10-803-2013,

593   2013.

594   Pujo-Pay, M., Conan, P., Oriol, L., Cornet-Barthaux, V., Falco, C., Ghiglione, J.-F., Goyet,

595   C., Moutin, T., and Prieur, L.: Integrated survey of elemental stoichiometry (C, N, P) from the

596   western to eastern Mediterranean Sea, Biogeosciences, 8, 883–899,

597   https://doi.org/10.5194/bg-8-883-2011, 2011.

598   Reygondeau, G., Guieu, C., Benedetti, F., Irisson, J.-O., Ayata, S.-D., Gasparini, S., and

599   Koubbi, P.: Biogeochemical regions of the Mediterranean Sea: An objective multidimensional

600   and multivariate environmental approach, Prog. Oceanogr., 151, 138–148,

601   http://dx.doi.org/10.1016/j.pocean.2016.11.001, 2017.

602   Sanchez-Vidal, A., Collier, R. W., Calafat, A., Fabres, J., and Canals, M.: Particulate barium

603   fluxes on the continental margin: a study from the Alboran Sea (Western Mediterranean),

604   Mar. Chem., 93, 105–117, https://doi.org/10.1016/j.marchem.2004.07.004, 2005.

605   Santinelli, C., Nannicini, L., and Seritti, A.: DOC dynamics in the meso and bathypelagic

606   layers of the Mediterranean Sea, Deep-Sea Res. Pt. II, 57, 1446–1459,

607   https://doi.org/10.1016/j.dsr2.2010.02.014, 2010.

608   Schlitzer, R.: Ocean Data View, GEO/ODV, available at: http://www.awi-bremerhaven.de/

609   (last access: 2 March 2021), 2002.

610   Simon, M. and Azam, F.: Protein content and protein synthesis rates of planktonic marine

611   bacteria, Mar. Ecol. Prog. Ser., 51, 201–213, 1989.

612   Stabholz, M., Durrieu de Madron, X., Canals, M., Khripounoff, A., Taupier-Letage, I., Testor,

613   P., Heussner, S., Kerhervé, P., Delsaut, N., Houpert, L., Lastras, G., and Dennielou, B.:

614   Impact of open-ocean convection on particle fluxes and sediment dynamics in the deep

615   margin of the Gulf of Lions, Biogeosciences, 10, 1097–1116, https://doi.org/10.5194/bg-10-

616   1097-2013, 2013.

Stange, P., Bach, L. T., Le Moigne, F. A. C., Taucher, J., Boxhammer, T., and Riebesell, U.: Quantifying the time lag between organic matter production and export in the surface ocean: Implications for estimates of export efficiency, Geophys. Res. Lett., 44, 268–276, https://doi.org/10.1002/2016GL070875, 2017.

Sternberg, E., Jeandel, C., Miquel, J.-C., Gasser, B., Souhaut, M., Arraes-Mescoff, R., and Francois, R.: Particulate barium fluxes and export production in the northwestern Mediterranean, Mar. Chem., 105, 281–295, https://doi.org/10.1016/j.marchem.2007.03.003, 2007.

Sternberg, E., Jeandel, C., Robin, E., and Souhaut, M.: Seasonal cycle of suspended barite in the mediterranean sea, Geochim. Cosmochim. Ac., 72, 4020–4034, https://doi.org/10.1016/j.gca.2008.05.043, 2008.

Stroobants, N., Dehairs, F., Goeyens, L., Vanderheijden, N., and Van Grieken, R.: Barite formation in the Southern Ocean water column, Mar. Chem., 35, 411–421, https://doi.org/10.1016/S0304-4203(09)90033-0, 1991.

Tamburini, C., Garcin, J., Ragot, M., and Bianchi, A.: Biopolymer hydrolysis and bacterial production under ambient hydrostatic pressure through a 2000m water column in the NW Mediterranean, Deep-Sea Res. Pt. I, 49, 2109–2123, https://doi.org/10.1016/S0967-0645(02)00030-9, 2002.

Tamburini, C., Boutrif, M., Garel, M., Colwell, R. R., and Deming, J. W.: Prokaryotic responses to hydrostatic pressure in the ocean – a review, Environ. Microbiol., 15, 1262–1274, https://doi.org/10.1111/1462-2920.12084, 2013.

Tanhua, T., Hainbucher, D., Cardin, V., Álvarez, M., Civitarese, G., McNichol, A. P., and Key, R. M.: Repeat hydrography in the Mediterranean Sea, data from the <i>Meteor</i> cruise 84/3 in 2011, Earth Syst. Sci. Data, 5, 289–294, https://doi.org/10.5194/essd-5-289-2013, 2013a.

642   Tanhua, T., Hainbucher, D., Schroeder, K., Cardin, V., Álvarez, M., and Civitarese, G.: The

643   Mediterranean Sea system: a review and an introduction to the special issue, Ocean Sci., 9,

644   789–803, https://doi.org/10.5194/os-9-789-2013, 2013b.

645   Taylor, S. R. and McLennan, S. M.: The continental crust: its composition and evolution,

646   Blackwell Scientific Publications, USA, 312 pp., 1985.

647   Van Wambeke, F., Taillandier, V., Deboeufs, K., Pulido-Villena, E., Dinasquet, J., Engel, A.,

648   Marañón, E., Ridame, C., and Guieu, C.: Influence of atmospheric deposition on

649   biogeochemical cycles in an oligotrophic ocean system, Biogeosciences, 2020, 1–51,

650   https://doi.org/10.5194/bg-2020-411, 2020.

651

652

653

654

655

656

657

658

659

660

661

662

663

664

665

666

667

668

669

670   Figure 1
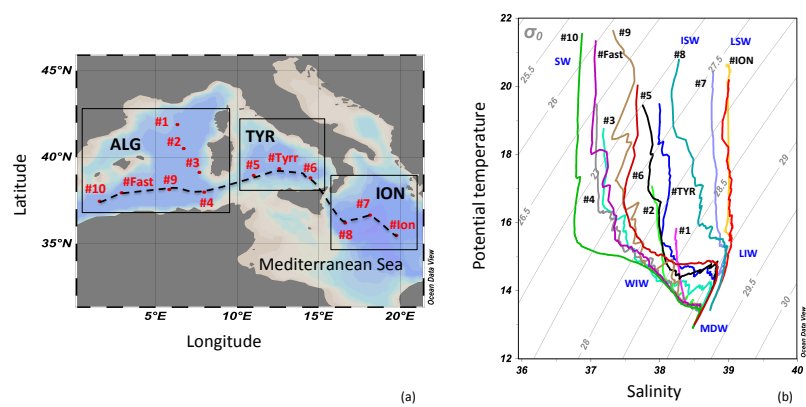
671

672

673

674

675

676   Figure 2
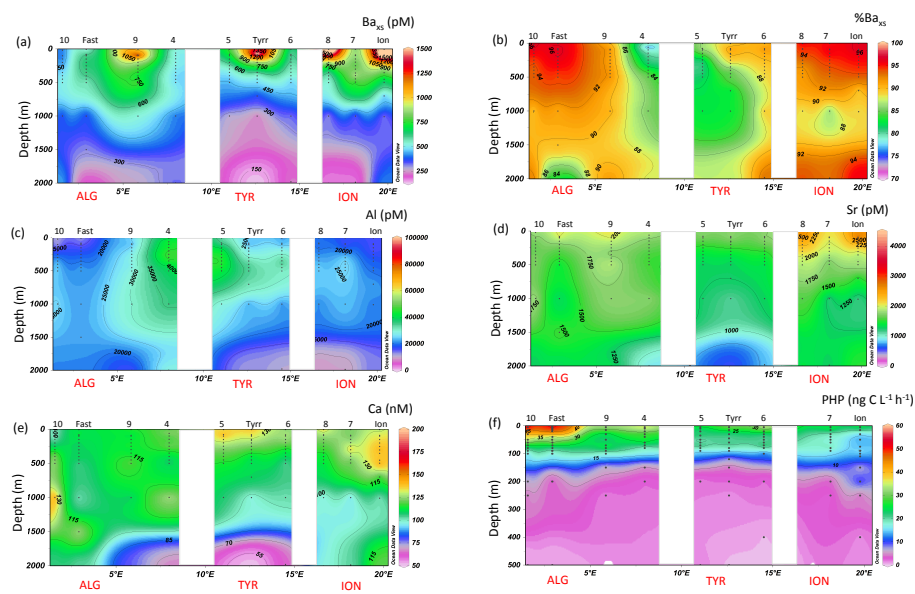
677

678

679

680   Figure 3
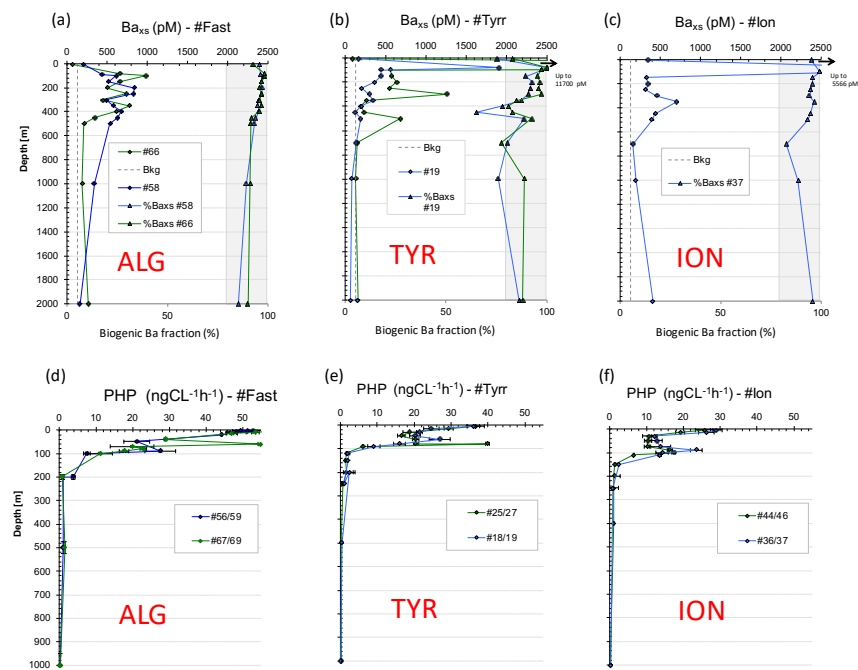
681

682

683

684   Figure 4
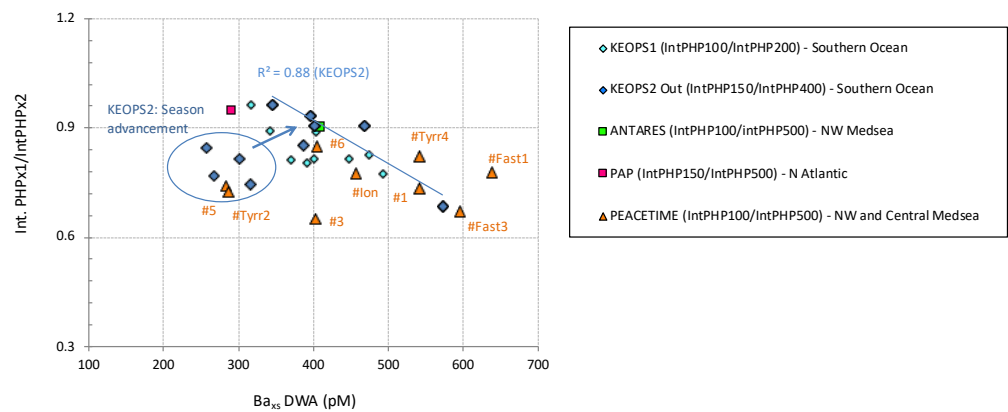
685

686

687

688

689   Figure 5
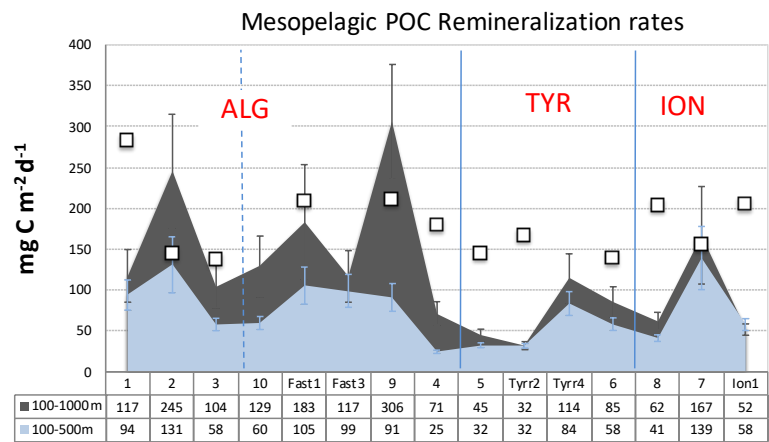
690

691

692

693   Table 1

Basin	Station #	Mesopelagic layer	DWA Ba_{xs} [pM]	MR [mg C m^{-2} d^{-1}]	MR Stnd error [%]
Algero-Provençal	1	upper	542	94	20
	1	entire	374	117	27
	2	upper	717	131	26
	2	entire	645	245	28
	3	upper	402	58	13
	3	entire	353	104	25
	4	upper	243	25	8
	4	entire	281	71	20
	9	upper	981	91	19
	9	entire	979	306	23
	Fast1	upper	638	105	21
	Fast1	entire	527	183	38
	Fast3	upper	596	99	20
	Fast3	entire	381	117	27
	10	upper	418	60	13
	10	entire	410	129	29
Tyrrhenian	5	upper	283	32	9
	5	entire	226	45	17
	Tyrr2	upper	284	32	9
	Tyrr2	entire	200	32	15
	Tyrr4	upper	542	84	17
	Tyrr4	entire	380	114	26
	6	upper	404	58	13
	6	entire	313	85	22
Ionian	7	upper	769	139	28
	7	entire	485	167	36
	ION	upper	456	58	13
	ION	entire	315	52	13
	8	upper	363	41	10
	8	entire	273	62	18

694